Influence of static pressure on the damping of pressure waves in rocket engine feed lines

Sebastian Klein, Tobias Traudt, Cristiano Bombardieri, Prof. Michael Oschwald

German Aerospace Center | Institut of Space Propulsion | Rocket Propulsion

Abstract

Water hammer pressure peaks are an important design parameter for rocket engine feedline systems. The emergency shutdown of an engine or the valve closure after the chill down procedure can lead to water hammer. To expand the knowledge of this phenomenon the influences from the static pressure on the damping constant will be investigated in this paper.

Water hammer damping experiments without cavitation have been executed at the **F**luid **T**ransient **T**est **F**acility (FTTF) at the DLR Lampoldshausen. The static pressure in the system was determined the only influence on the damping constant.

1 INTRODUCTION

Water hammer phenomena are of great interest in the field of rocket engineering. Closing a valve rapidly to shut down a rocket engine or stop the chill down procedure can generate high amplitude pressure waves in the feed line system and damage it. This caused the loss of the N1 rocket at its 4th flight [1]. Therefore, this phenomenon has a significant influence on the design of the feeding system.

Water Hammer phenomena have been investigated since the late 19th century. Joukowsky was one of the first who studied this field. A very detailed overview about research activities in theory and practice can be found in Ref. [2] and [3]. Fluid structure interaction has been studied in Ref. [4]. Most of these investigations were performed with water.

In Ref. [5] the authors distinguish between the flow behavior in elastic and plastic pipes. They presented a formula to calculate the piezometric head for both pipes. By using two factors (K_1, K_2) the calculated damping function matches well with the experimental data. The static pressure is not an issue for both factors. Good agreement of unsteady friction models for the first $0.4s$ are also seen in Ref. [6]. Several friction models were part of their study and no model includes the pressure as a parameter.

Several water hammer tests with and without cavitation have been performed at the FTTF at DLR Lampoldshausen [7] [8]. The water hammer was created by using a fast closing valve to stop a steady flow. In Ref. [8] the authors showed tests in which the 2nd peak is up to 25% higher than the 1st peak. They used an optical access to investigate occurring cavitation phenomena. A method to track cavitation bubbles in the flow was presented. Intermediate spikes were found at the cavitation time range, the first spike is accompanied by reversal of the flow direction.

Unpublished priming tests with cavitation at the same test bench showed that the damping constant δ changes with the static pressure [9].

The static pressure is the pressure in the upstream tank prior to valve closing. To find out if this behavior is related to the occurrence of cavitation, water hammer tests at a static pressure range from $p = 20 - 48$ bar without cavitation will be used to investigate the influence of the static pressure on the damping and it will be shown that a higher pressure correlates with a lower damping constant δ. Furthermore an empirical approach to calculate $\delta(p)$ will be presented.

2 TEST BENCH

A schematic overview of the M3.5 is shown in Figure 1. The fluid flows through the test section from the high pressure (HP) to the low pressure (LP) tank. By closing the fast acting valve the water hammer is created.

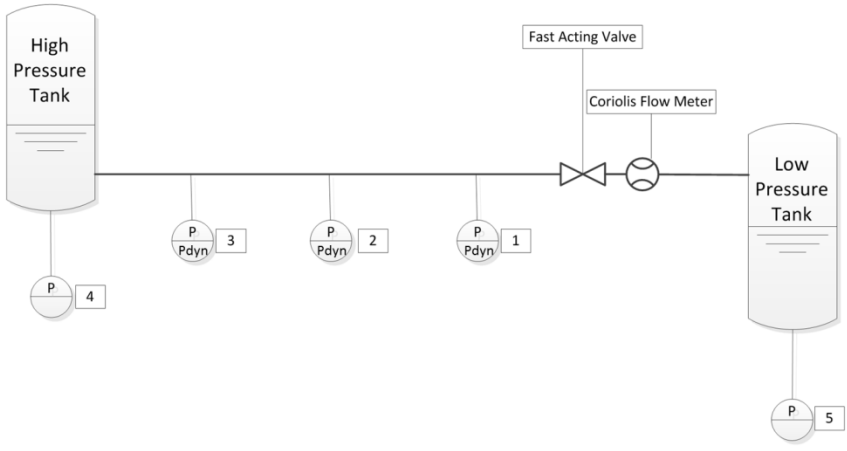

Figure 1: Schematic test bench M3.5

Both tanks are pressurized by gaseous nitrogen. This creates a stationary flow in the pipeline. The pressure is constant within $\pm$ 0.4% because it is regulated automatically.

A CAD model of the test bench is given in Figure 2. The main element of the test section is a one and a half twin spiral with a diameter of 1.25 m. The spiral contains an upward slope of ~1°. The test bench is made of stainless steel of grade 1.4541. The most important geometry parameters and sensor positions can be found in Table 1. Static pressure sensors of the type Kistler $4043A-100$ and dynamic pressure sensors of type Kistler $601A$ are mounted at position $1, 2$ and 3 (Figure 1).

Table 1: Dimensions of the test bench

Description	Symbol	Length
Test section length	l_{ts}	7.671 m
Test section inner pipe diameter	$d_{i,ts}$	19 mm
Test section wall thickness	e_{ts}	1.5 mm
Sensor 1distance from valve seat	l_1	0.3 m
Sensor 2 distance from valve seat	l_2	6.9 m
Sensor 3 distance from valve seat	l_3	7.6 m

The fast closing valve is a pneumatically operated coaxial valve. The valve closing time can be varied by changing the working pressure. The opening of the valve can be tracked by using the internal position encoder. A Coriolis flow meter is mounted downstream the coaxial valve. Above the fast closing valve is the valves pressureization system which can be run with nitrogen or helium. Furthermore this system is used to purge the valve after each test.

A detailed description of the test procedure and a comparison between theoretical predicted and experimental observed pressure peaks at the M3.5 can be found in [7]. The test section is purged and the water is stored overnight to make sure that no gas bubbles are left in the water. After ~4.5 s the flow is steady and then stopped by closing the fast acting valve. Before the next test the fast acting valve is purged by its own purging valve to remove any entrapped nitrogen.

Further information about the FTTF can be found in Ref. [7].

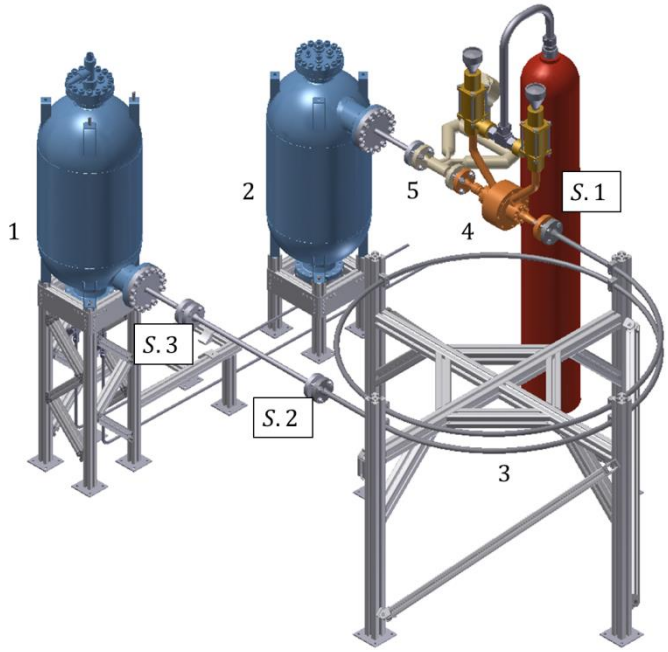

Figure 2: CAD model of the FTTF – High pressure tank [HP] (1), Low pressure tank [LP] (2), Test section (3), Fast closing axial valve with pressurization system (4), Coriolis flow meter (5), Sensor position 1-3 (S.1 – S.3)

3 RESULTS

3.1 Static pressure sensors

Water hammer tests have been performed over a pressure range from $p_{HP} = 20 - 48$ bar. Since the topic of interest is the behavior of damping in relation to the static pressure tank p_{HP}, only tests without cavitation will be considered. In this section only data from the static sensors are evaluated. An additional investigation of the dynamic pressure sensors can be found in section 3.2. The sampling rate for the static pressure sensors is $f_{static} = 10$ kHz.

The initial conditions and other important parameters for all investigated cases can be found in Table 2. In detail it concerns the pressure in both tanks P_{HP} and P_{LP}, the resulting pressure difference ΔP, the mass flow $\dot{m}$, the valve closing time Δt_{valve} und the flow velocity v. As seen in [7] the speed of sound in the water is $c = 1392\, m/s$. The arithmetic average roughness of the pipe was measured $R_a = 1.0363$ µm with a maximal roughness (valley to peak) of $R_{max} = 13.8$ µm for all cases.

Table 2: Initial Conditions

Number		P_{HP} [bar	P_{LP} [bar]	ΔP [bar]	$\dot{m}$ [$\frac{\text{kg}}{\text{s}}$]	Δt_{valve} [ms]	v [$\frac{\text{m}}{\text{s}}$]
20140226	19	41,28	40,08	1,20	0,57	15,30	2,01
	20	41,35	40,21	1,14	0,55	17,30	1,92
	21	41,29	40,20	1,09	0,53	17,60	1,89
	22	41,90	40,42	1,48	0,67	17,40	2,35
	23	41,92	40,43	1,49	0,67	17,40	2,35
	24	41,95	40,51	1,44	0,65	17,10	2,28
20140227	2	46,73	46,09	0,63	0,37	17,60	1,29
	3	46,74	46,11	0,63	0,36	17,80	1,28
	4	47,28	46,35	0,93	0,50	18,00	1,77
	5	47,31	46,37	0,94	0,50	17,80	1,75
	6	47,32	46,35	0,98	0,51	17,70	1,79
	7	47,82	46,62	1,20	0,59	17,60	2,06
	8	47,85	46,62	1,22	0,59	17,40	2,09
	9	47,83	46,63	1,20	0,58	17,40	2,06
20140318	27	32,79	31,10	1,69	0,73	17,70	2,57
	28	32,78	31,32	1,46	0,66	17,90	2,32
	29	32,80	31,35	1,46	0,65	18,10	2,31
	30	30,76	30,34	0,42	0,20	18,10	0,72
	31	30,78	30,35	0,43	0,20	18,10	0,69
20140321	24	20,57	20,14	0,42	0,33	17,40	1,16
	25	20,57	20,25	0,33	0,26	17,60	0,91
	26	20,57	20,32	0,25	0,22	17,80	0,76
20140910	18	31,30	30,20	0,90	0,60	22,10	2,11
20140930	19	30,38	29,83	0,31	0,37	11,60	1,31
	20	30,39	29,89	0,26	0,36	11,40	1,27

The pressure profiles at both ends of the pressure range are shown in Figure 3 ($p_{HP} = 20$ bar) and Figure 4 ($p_{HP} = 48$ bar). As expected, the water hammer profile is most pronounced at position 1. Therefore this sensor will be used for the following damping analysis. Furthermore, both tests show phenomenologically the same characteristics. It can be suspected that the damping is different. The damping at the high pressure profile seems to be lower than at the low pressure profile.

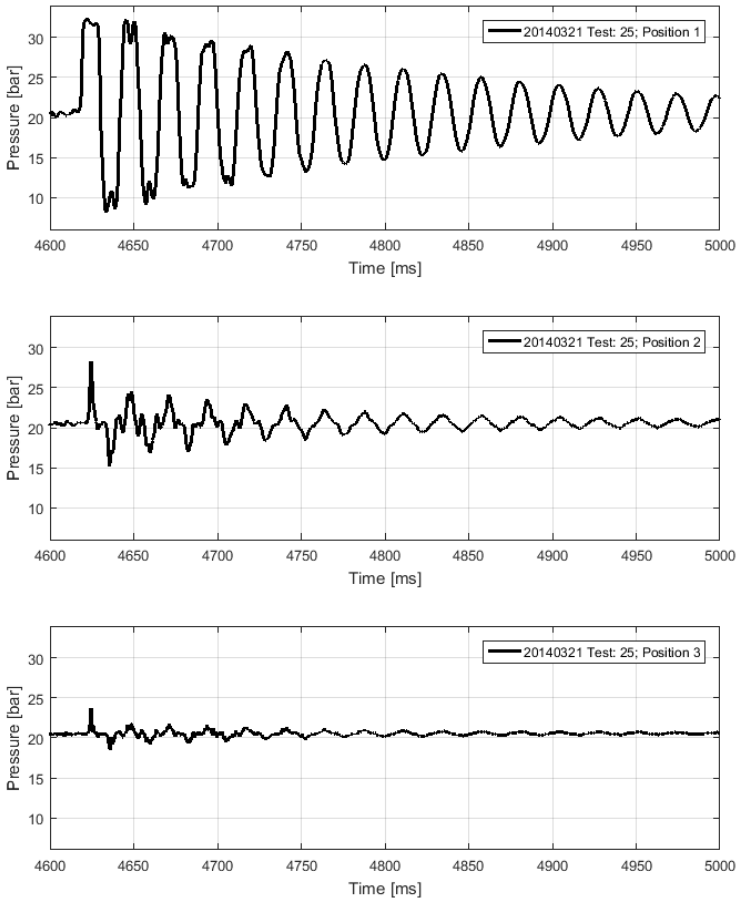

Figure 3: Pressure profiles for $p_{HP} = 20$ bar, static pressure sensors

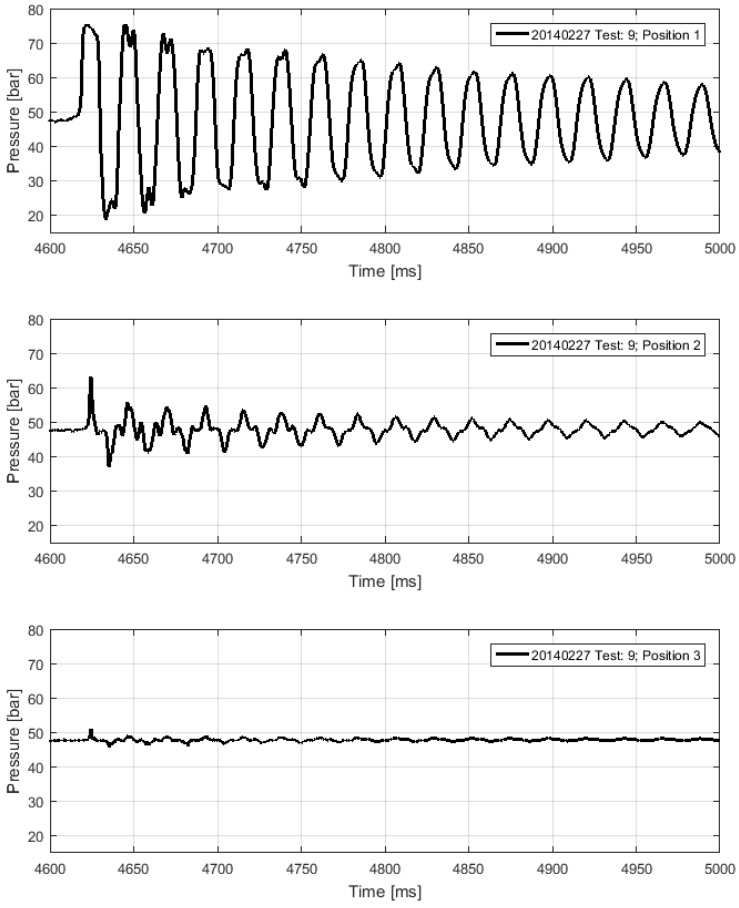

Figure 4: Pressure profiles for $p_{HP} = 48$ bar, static pressure sensors

The envelope functions of the experimental pressure data (Figure 3, Figure 4) at position 1, scaled to p_{HP} are shown in Figure 5. To calculate these lines the *envelope* function of matlab is used. The functions parameter was chosen so that the *envelope* function only cross the pressure peaks. The data is cut prior to the first peak. Both first peaks are nearly the same height, which makes it easier to compare both runs. The difference between those graphs leads to the hypothesis that the decay constant δ is a function of the static pressure $\delta = \delta(p_{HP})$.

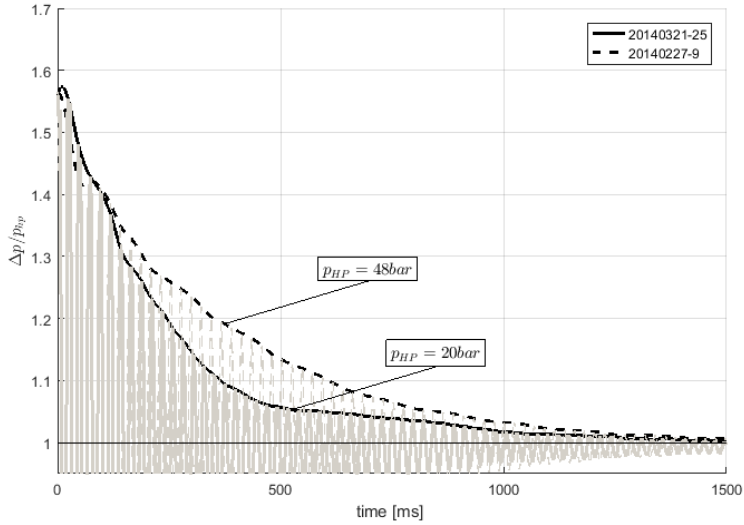

Figure 5: Envelope functions of the experimental pressure data scaled to p_{HP}

To investigate this hypothesis the envelope function will be compared to the damping function:

$$y(t) = \hat{y}\, e^{-\delta t} \qquad 1$$

Where $\hat{y}$ is the amplitude of the first (and highest) peak, δ is the decay constant and t the time. This is the damping function for an oscillation around 0, while the graphs in Figure 5 are oscillations around 1 (due to the normalization). Hence a shift of 1 in the y direction is needed.

To calculate δ the envelope function is fitted by the following approach:

$$f(t) = a\, e^{bt} + c\, e^{dt} \qquad 2$$

Where a, b, c, d are free parameters of function $f(t)$. For all tests $d = 0$ with an accuracy of $5 * 10^{-5}$ and $c = 1$ with an accuracy of $\pm 2\%$. This leads to:

$$(c \approx 1)e^{(d \approx 0)t} \approx 1 \qquad 3$$

With those two values the second term of equation **2** can be considered as a shift along the y-axis by 1.

Parameter a over the max deviation $(\Delta p/p_{PH}) - 1$ is shown in Figure 6. Both values are nearly equal, therefore Parameter a can be considered as the max amplitude $\hat{y}$.

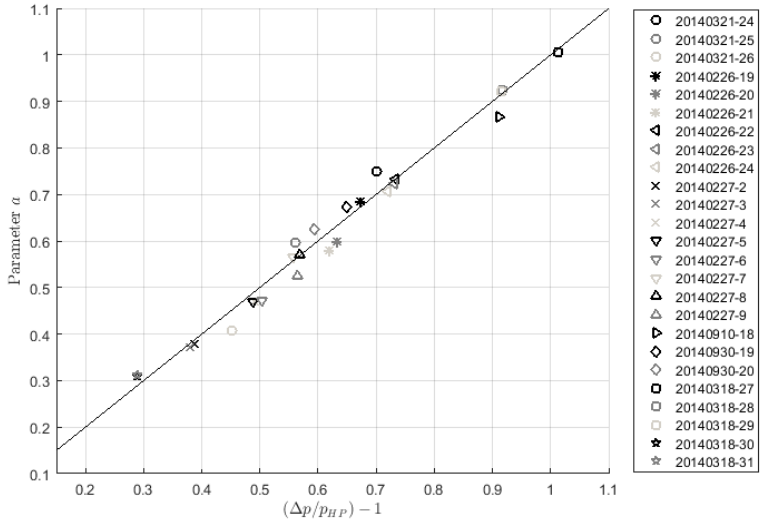

Figure 6: Parameter a over the maximum deviation $(\Delta p/p_{PH}) - 1$

After the parameters a, c, d have been determined, this leads to $b = -\delta$. The damping constant δ for different flow velocities v is shown in Figure 7. There is no direct correlation noticeable.

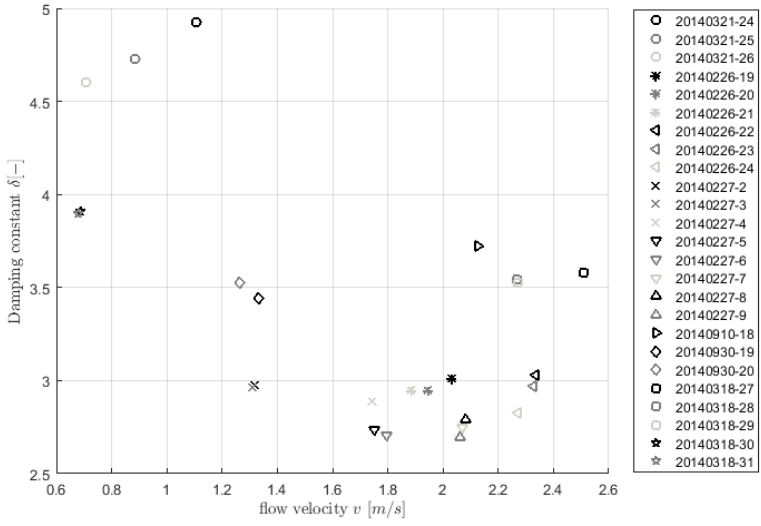

Figure 7: Influence of the flow velocity v on the damping constant δ

The damping constant δ for different static pressures p_{HP} is shown in Figure 8. It is easy to see a correlation between these parameters. The black line is a $2nd$ grad polynomial fit function (best fit in a least-squares sense).

$$\delta(p) = 0.0019 * p^2 - 0.1999 * p + 8.0857 \qquad 4$$

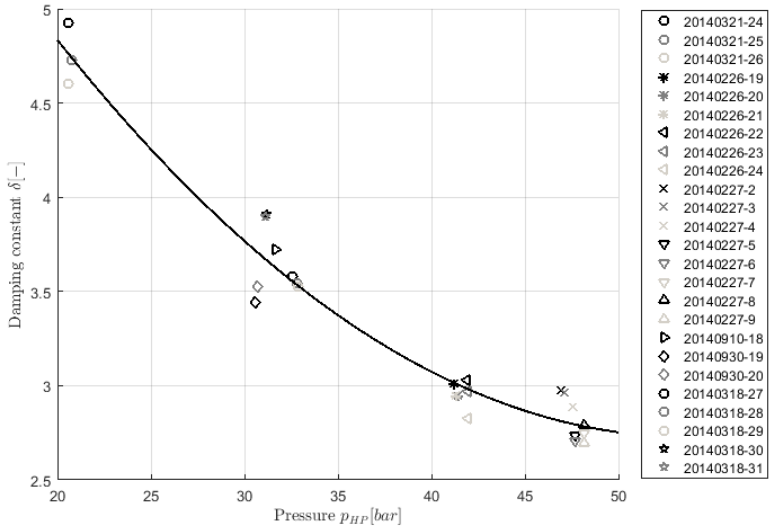

Figure 8: Influence of the static pressure p_{HP} on the damping constant δ, Position 1

Figure 9 shows δ over p at position 2, Figure 10 shows position 3. It is not possible to see the same trend at both positions. Besides all uncertainties, the damping constant δ tends to be higher at sensor positions more downstream.

To understand this correlation the damping process must be understood. Two effects are responsible for the damping in the system, fluid structure interaction (FSI) and friction (inner friction and wall friction). The following fluid properties are almost constant over all studied tests and do not explain the observed behavior. *Temperature*, *density*, *speed of sound*, *kinematic viscosity*, *compressibility* and the *inner energy*. Therefore it seems that the inner friction does not have any influence on the damping constant δ. A correlation between δ and the *mass flow* or the *velocity* prior to valve closing have not been found.

Unsteady friction models described in Ref. [9] and Ref. [6] do not include pressure dependence. In Ref. [10] the authors described a method to calculate the elementary unit weight friction force, which does not depend on the pressure also. Hence these models should predict an equal dissipation of friction energy for different pressures.

Since the experimental setup is equal in all tests and if our assumptions above are correct, the energy (friction) dissipates from the system should be equal. This should lead to constant damping behavior for different pressures, which does not match with the experimental observation. A possible explanation could be that the pressure has an influence on the wall friction. Furthermore the FSI could have an influence on the

damping. The potential energy rises if p_{HP} rises, which leads to an oscillation on a higher potential energy level.

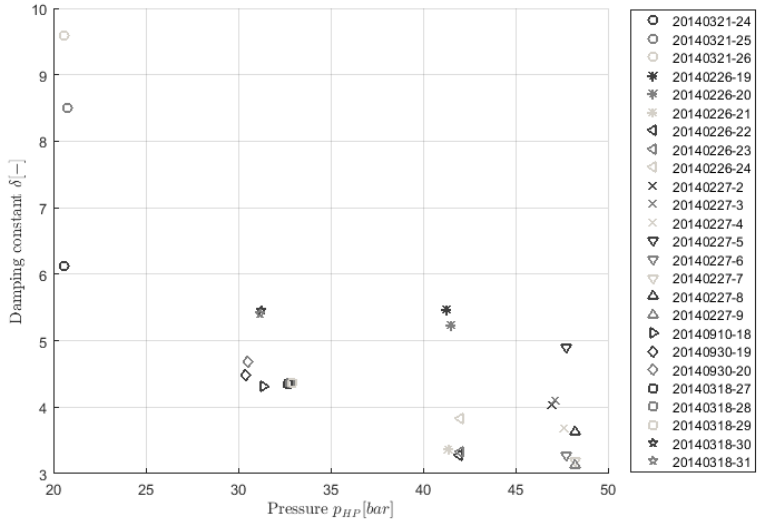

Figure 9: Influence of the static pressure p_{HP} on the damping constant δ, Position 2

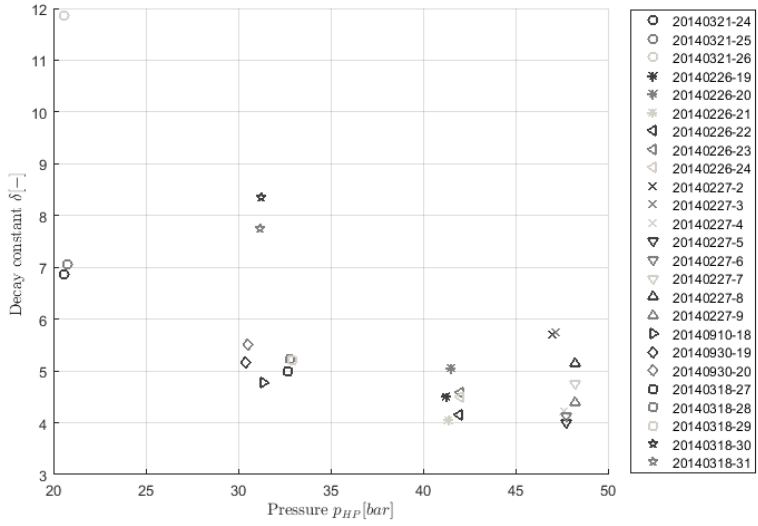

Figure 10: Influence of the static pressure p_{HP} on the damping constant δ, Position 3

3.2 Dynamic pressure sensors

Dynamic pressure sensors measure only relative pressure fluctuations using a very high sampling rate ($f_{dyn} = 150$ kHz). In case of water hammer tests this leads to an oscillation around zero (Figure 11). Besides this shift in mean pressure the history of the graph is nearly identical to Figure 3.

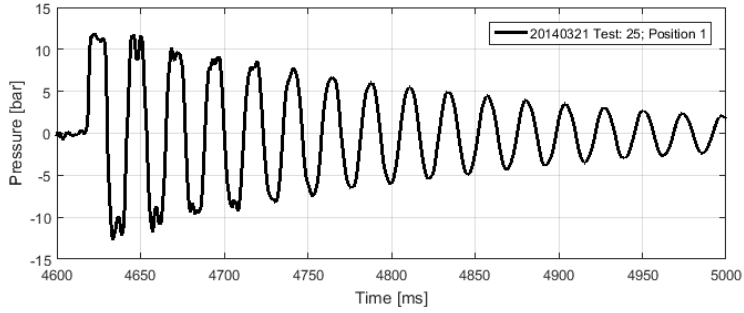

Figure 11: Pressure profiles for $p_{HP} = 20$ bar, dynamic pressure sensors

The aforementioned approach (equation 1) to calculate the damping constant δ can therefore be simplified to $f(t) = a\, e^{bt}$. Equivalent to Figure 8, δ applied over p_{HP} for dynamic pressure sensors is shown in Figure 12. It was not possible to find a valid fit function with this approach for three runs, therefore they are not displayed.

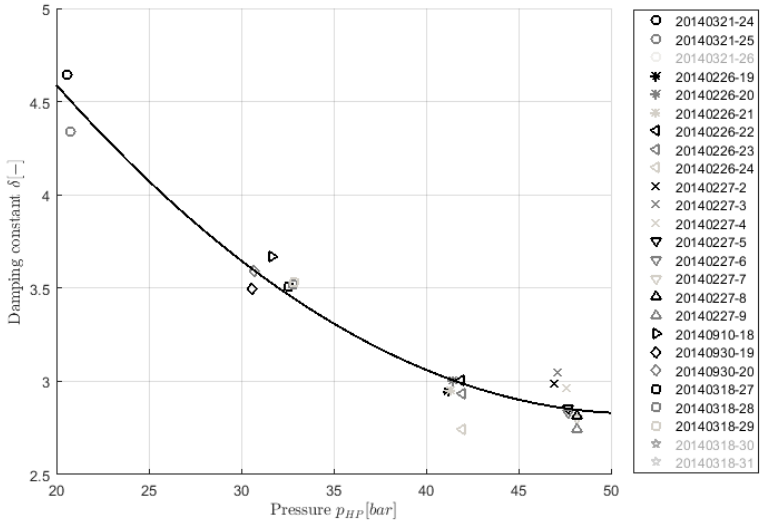

Figure 12: Damping constant δ over pressure p_{HP}, Pos. 1, Dynamic pressure sensor

A similar dependence to equation 4 can be observed for $\delta(p)$ in Figure 12:

$$\delta(p) = 0.0018 * p^2 - 0.1832 * p + 7.5408 \quad (5)$$

The deviation between equation 4 and equation 5 can be explained by the different method of determining δ. Nevertheless, these functions are very similar.

Like the static pressure sensors, the dynamic pressure sensors also do not provide a significant dependence of $\delta$and p_{HP} at positions 2 and 3.

4 CONCLUSION AND OUTLOOK

Several tests without cavitation have been investigated. The tests took place in a pressure range from 20 bar to 48 bar, the maximum pressure peak was in a range from 31% to 100% of the static pressure p_{HP}. All tests have been performed at the same test bench under the same conditions. The envelope function of the pressure signal was fitted by an exponential function. The damping constants δ have been identified and compared to each other. The static pressure has been identified as a major influence on δ. An empirical approach was given for δ as a function of p. This dependence was found in the data of static and dynamic pressure sensors at position 1 but not at position 2 or 3.

Since we could not give an explanation for the pressure dependence of the damping, we suggest further studies to focus on the wall friction and the fluid structure interaction.

It is of interest if the damping behaves the same in water hammer tests with cavitation, these tests will be evaluated in future works. After this the tests will be repeated with LN2 and LOX to compare cryogenic and non-cryogenic fluids. LOX is the real fluid for rocket engine feed line systems. Therefore it is of great interest. Among other it will be investigated how the pressure influence of the damping constant will change for cryogenic fluids. This work focused on the experimental side, the comparison to numerical results will be done in future works. The authors consider these data as a valuable test case for numerical work.

5 REFERENCES

[1] C. Lardier, „The soviet manned lunar program N1-L3,“ *Acta Astronautica,* Bd. 142, pp. 184-192, 2018.

[2] A. Bergant, A. R. Simpson und A. S. Tijsseling, „Water hammer with column separation: A historical review,“ *Journal of Fluids and Structures,* Bd. 22, pp. 135-171, 2006.

[3] M. S. Ghidaoui, M. Zhao, D. A. McInnis und D. H. Axworthy, „A Review of Water Hammer Theory and Practice," *ASME,* Bd. 58, pp. 49-76, 2005.

[4] A. S. Tijsseling, „Fluid Structure Interaction in Liquid-Filled Pipe Systems: A Review," *Journal of Fluids and Structures,* Bd. 10, pp. 109-146, 1996.

[5] H. Ramos, D. Covas, A. Borga und D. Loureiro, „Surge damping analysis in pipe systems: modelling and experiments," *Journal of Hydraulic Research,* Bd. 42, pp. 413-425, 1 2004.

[6] H. Shamloo, R. Norooz und M. Mousavifard, „A review of one-dimensional unsteady friction models for transient pipe flow," *Science journal (CSJ),* Bd. 36, 2015.

[7] T. Traudt, C. Bombardieri und C. Manfletti, „Influences on Water Hammer Wave Shape an Experimental Study," in *63. Deutscher Luft- und Raumfahrtkongress, Augsburg Germany,* 2014.

[8] T. Traudt, C. Bombardieri und C. Manfletti, „High Speed Imaging of Water Hammer with Column Separation," in *Pressure Surge Conference, Dublin,* 2015.

[9] C. Bombardieri, „Experimental Investigation of the Filling Process in Evacuated Spacecraft Propulsion System Feedlines," 2018.

[10] B. Brunone, U. M. Golia und M. Greco, „Effects of Two-Dimensionality on Pipe Transients Modeling," *Journal of Hydraulic Engineering,* 1995.